Available online at www.sciencedirect.com

ScienceDirect

Physics Procedia 83 (2016) 864 – 873

Physics Procedia

9th International Conference on Photonic Technologies - LANE 2016

Reduction of the residual porosity in parts manufactured by selective laser melting using skywriting and high focus offset strategies

A.M. Mancisidor[a,]*, F. Garciandia[a], M. San Sebastian[a], P. Álvarez[a], J. Díaz[b], I. Unanue[b]

[a]*IK4-Lortek, Arranomendi kalea 4A, 20240 Ordizia, Spain*
[b]*ITP, Parque Tecnologico nº 300, 48170 Zamudio, Spain*

Abstract

Residual porosity is observed in Inconel 718 samples manufactured by SLM within the optimum process window regardless the process parameters whose origin has been directly related to the starting and finishing of the laser scanning tracks. This porosity is concentrated preferentially in overlaps of fields (stripes and chessboard strategies) and borders. Location of pores has been demonstrated on long stripes, where laser stops only at borders, not in the hatch. It has been concluded that porosity is due to a high interaction time of the laser with powder which increases the energy in those points. Two different strategies have been validated to reduce this effect and thus diminish porosity. These strategies are the skywriting function, where the laser is switched off during the accelerating and decelerating portions and to increase the focus offset. The defocusing strategy is not as effective as the skywriting reducing the residual porosity.

Peer-review under responsibility of the Bayerisches Laserzentrum GmbH

Keywords: Residual porosity; skywriting; selective laser melting; focus offset

1. Introduction

Selective Laser Melting (SLM) is an Additive Manufacturing technology where components are manufactured layer by layer, scanning selectively a powder bed using a high-power laser beam. The laser energy is intense enough to permit full melting (welding) of the particles to form a solid metal (Aboulkhair et al. 2014; Averyanova et al.

* Corresponding author. Tel.: +34-943-882-303 ; fax: +34-943-884-345 .
E-mail address: ammancisidor@lortek.es

Peer-review under responsibility of the Bayerisches Laserzentrum GmbH
doi:10.1016/j.phpro.2016.08.090

2010). The principal advantage of SLM is the potential to create complex components for aeronautic, automotive, medical, electronic or tooling industry that would be difficult or impossible to produce using conventional manufacturing techniques (Averyanova et al. 2010; Gong et al. 2012). SLM process is controlled by a set of parameters that have an important impact on mechanical properties. Some of these parameters are associated with material factors which are characteristic of the material and are not controllable such as thermal conductivity, absorption coefficient, melting point and coefficient of thermal expansion. The parameters that are largely controllable are correlated with the process and can be classified as laser, scan, powder and temperature-related. The most important parameters involved in the process are laser power, scanning speed, hatch spacing and layer thickness (Aboulkhair et al. 2014; Kurzynowski et al. 2012). Several investigations consider these parameters to optimize part density (Buchbinder et al. 2011; Louvis et al. 2011; Kempen et al. 2011; Olakanmi 2013). Other studies can be found which are focused on designing scanning strategy to minimize porosity of produced parts (Aboulkhair et al. 2014).

Each metal alloy can be processed within a energy density process window which gives rise to defect free structure and the highest relative density values. The generation of porosity is caused by an excesive energy input which creates a less stable large melt pool, resulting in the balling effect. On the other hand, insufficient energy input which is not capable of fully molten the successive scan tracks, can give rise to lack of fusion defects (Gong 2013; Thijs et al. 2010).

In this study, the influence of skywriting function and focal offset on residual porosity obtained in Inconel 718 samples manufactured by SLM has been investigated. Skywriting is a function which compensates the inertia of scanning mirrors and enables the acceleration of mirrors before the beginning of laser exposure. The influence of skywriting on dimensional accuracy and surface roughness has been previously investigated (Moylan et al. 2014), but there are no evidences of the influence of this function on hatch relative density and residual porosity. It must be noted that scanning start and stop events can be given in the hatch of the parts if chessboard or short stripes scanning patterns are selected. These scanning patterns have a practical interest because they can reduce distortions and residual stresses (Alvarez et al. 2016). On the other hand, modifying the focus of the beam, i.e, changing the focal point from the upper working surface, the spot size and energy distribution can be changed. Therefore, the powder-laser interaction will be different both during the acceleration and decelaration steps and during constant scanning speed.

2. Experimental procedure

The powder used in this study was Inconel 718 nickel superalloy supplied by LPW Tech. Ltd. and produced by argon gas atomization with a particle size distribution between 10-45 μm and spherical morphology. The composition is specified in Table 1.

Table 1. Chemical composition of Inconel 718 powder.

Powder	% Ni	% Cr	% Co	% C	% Mo	% Al	% Ti	% Fe	% Nb+Ta	% Mn
IN718	52.88	19.11	0.03	0.04	3.1	0.50	0.95	Bal	5.03	<0.10

A first set of trials was performed for the definition of the process window. Simple samples, cubes of 10 mm x 10 mm x 10 mm, were manufactured by SLM. These specimens were built in a system developed by SLM Solutions (model SLM 280HL). This machine is equipped with 400 W fiber laser and works within a protective argon atmosphere. Samples were produced at a laser power (*P)* of 200 W and beam focused close to the surface. The scanning speed (*v)* was varied from 600 mm/s to 1100 mm/s modifying the energy density applied to the samples.

After obtaining the process window of the material, the influence of skywriting function and defocus on residual porosity was investigated. The focus offset was varied from close to surface up to 12 mm keeping the skywriting function disabled, and on the other hand, the skywriting function was enabled keeping the original focus close to the surface. These two strategies diminish the energy density, due to an increase of the scanning surface with high focus offset or power reduction in critical points with skywriting. In the case of high focus offset values, lower scanning speeds were also employed to avoid defect generation due to too low energy density.

In both cases, two scanning strategies (the order and orientation of generated micro-welds inside a layer) were investigated, chessboard pattern with displaced islands and stripes. Islands were moved a given value in x and y direction from layer to layer (Fig. 1a). In the stripe configuration the deposition direction is not changed in the same layer but a certain angle is shifted from layer to layer (Fig. 1b).

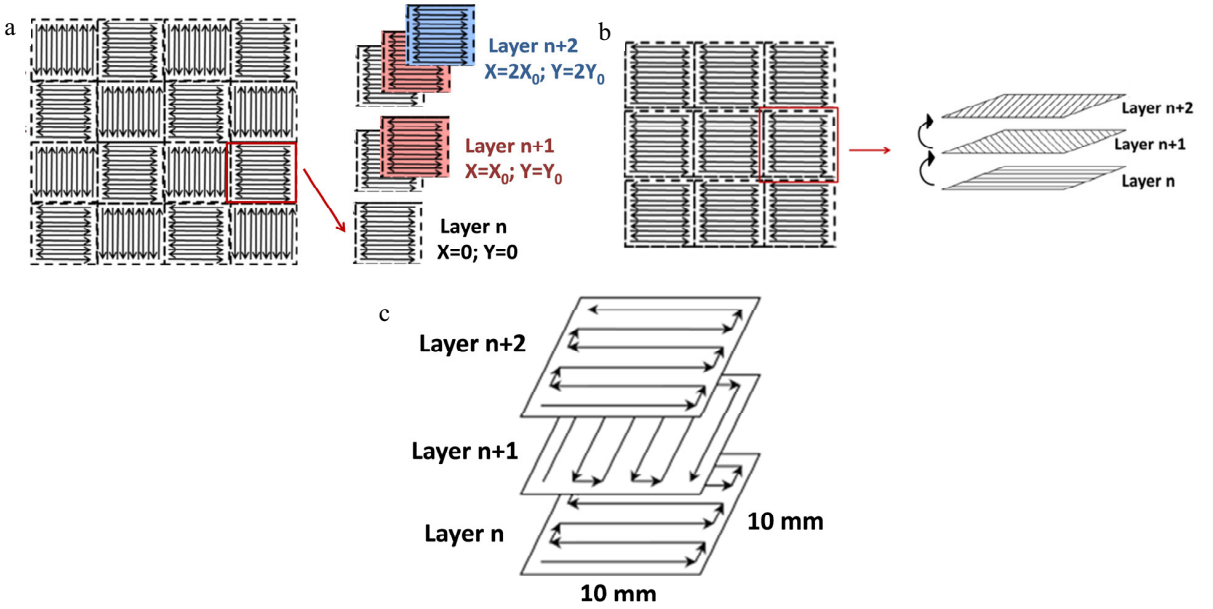

Fig. 1. Representation of scanning strategies. (a) Chessboard; (b) Stripes; (c) Long stripes.

The manufactured cubes were characterized in terms of relative density, internal defects and microstructure. Relative density was determined in sections perpendicular to the building direction (in XY planes) by means of optical microscope (GX51 Olympus) and with the help of the image analysis software AnalySISdocu. Relative density was determined in the zones with greater concentration of pores. Microstructure was studied both in transversal and longitudinal directions, identifying the location of pores. For that, the samples were prepared following the usual metallographic procedure and were etched using 6 ml H_2O + 60 ml HCl + 6 g $CuCl_2$ reactant before performing optical microscopy examination.

3. Results and discussion

3.1. Relative density and process window

SLM process window of Inconel 718 was defined keeping the skywriting function disabled and focusing the beam close to the surface. Fig. 2 shows the correlation of the obtained relative density of the material with applied volumetric energy density. Energy density values were calculated from Ec. 1. Relative densities above 99.5% were obtained for energy densities between 55 J/mm^3 and 93 J/mm^3. Similarly to several authors (Aboulkhair et al. 2014; Kempen et al. 2011), at low energy densities, that is, at high scanning speeds, lack of fusion defects are appreciable due to an incomplete melting of powder particles. However, at high energy densities and thus low scanning speeds, porosity is observed. This porosity has been related to the trapping of surrounding gases or powder occluded gases within the melt pool (Dahotre & Harimkar 2008; Xiao & Zhang 2014). It can also come from vaporation of metal. A reduction of relative density at high energy densities has not been observed in this study and it would have been necessary to increase even more the energy density. In (Jia & Gu 2014), lower density was obtained (98.4%) applying the same linear laser energy density as in this study (330 J/m).

Taking into account that a remaining residual porosity was obtained within the process window and irrespectively of the process parameters, a deeper analysis was performed to characterize this porosity and determine its origin.

Micrographs of samples manufactured at 55 and 90 J/mm^3 were analysed without etching (Fig. 3 (a) and (b)). In both micrographs porosity was observed with the peculiarity that pores were apparently aligned. In addition, this porosity was irrespective of the employed processing parameters and scanning strategy, chessboard or stripes. Moreover, the generation of both spherical and large size pores, some of them reaching 60 µm, was atributted to high local energy densities (Gu et al. 2013). Other hypothesis which could be responsible of the remaining porosity such as internal porosity of powder, powder humidity and spot size were discarded due to their random nature which cannot explain the observed pore alignement. Special drying procedure was applied to raw Inconel 718 powder (Fig. 3 (c)) in order to reduce its humidity. The humidity was measured by hygroscope obtaining always values below 10%. This level of humidity is considered appropriate to process the powder by SLM and to achieve uniform powder layers. The spot size was in the range of 80-120 µm according to the machine manufacturer, considered as a normal value.

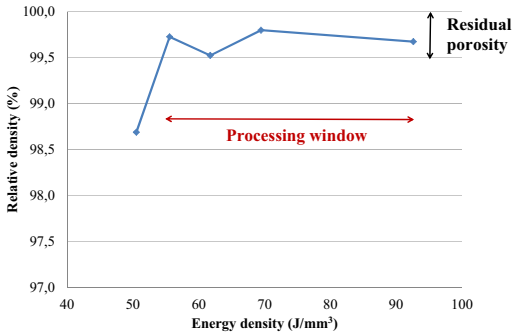

$$E = \frac{P}{v \cdot h \cdot t} \quad (1)$$

E = energy density
P = laser power
v = laser scanning speed
h = hatch spacing
t = layer thickness

Fig. 2. Evolution of relative density of sample manufactured by SLM with applied laser energy density and energy density equation.

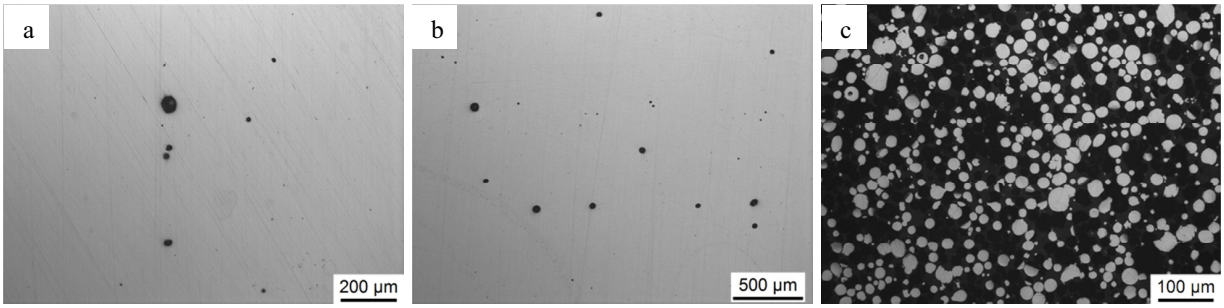

Fig. 3. Micrographs of samples manufactured within the optimum process window showing aligned porosity. (a) Chessboard strategy; (b) Stripes strategy. (c) Internal porosity of raw Inconel 718 powder.

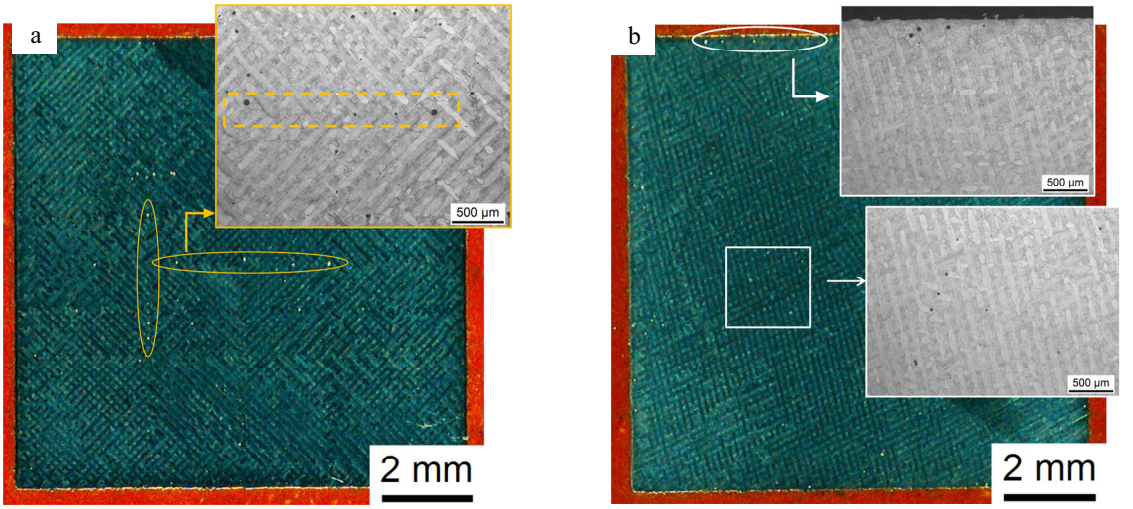

Fig. 4. Microstructures of etched samples (a) chessboard strategy; (b) stripe strategy.

Samples were chemically etched in order to find out the location of the aligned residual porosity. Micrographs of Fig. 4, where the whole area of the sample is shown, reveal that porosity was located preferentially in overlaps of scanning fields as well as in borders of the samples. Note that the bright points highlighted in Fig. 4 are pores with a lower magnification than in related micrographs. In Fig. 4 (a), where the black and white fields of chessboard strategy are clearly marked, it can be affirmed that pores were located in their mutual intersections or overlaps (marked with yellow circles). Moreover, in Fig. 4 (b) a concentration of pores in borders was noticed (marked with white circles) at stripe overlaps. Higher magnification images of these areas show more clearly the overlaps of fields (dashed yellow rectangle) and location of porosity (black points). These specific places where porosity is observed matches with starting and finishing of the laser scanning tracks.

3.2. Origin of the residual porosity

In order to fully demonstrate that observed residual porosity is directly linked to the starting and finishing of the laser scanning tracks and discard any other factors, additional cubes were manufactured, avoiding start and stops events in the hatch, that is using long stripes along the whole part length. Stripe strategy was selected with a stripe length of 10 mm, thus, equal to the length of the side of the cube. In this way, the laser only stopped at borders, never in the hatch. It is worth noting that these cubes were laser scanned without borders or contours in order to avoid any influence of border parameters in porosity near the subsurface. In Fig. 1 (c), an scheme of applied scanning strategy is illustrated.

Fig. 5 shows the resulting micrographs in which a hatch almost without porosity was achieved (99.98% relative density), whereas a concentration of pores in borders was observed. The same powder and process parameters like before were used. According to these results, it is fully concluded that the residual porosity observed in samples included in section 3.1, is a concequence of the laser start and stop events. At these points, the scanning speed reaches a extremely low value, that it could be zero during very short period of time, giving rise to long interation time between the laser and the powder. In other words, the energy density is exceptionally high causing the evaporation of the powder and generating porosity. (Chivel 2014) investigated the ablation phenomena with droplets ejection when the melt is overheated in SLM process.

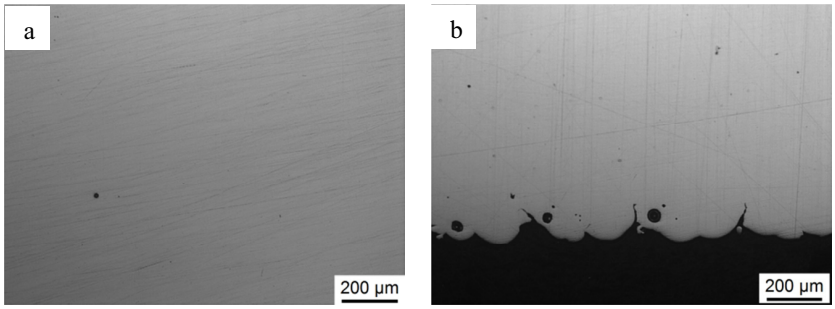

Fig. 5. Micrographs of samples manufactured with long stripes showing a hatch almost free of porosity and a concentration of pores in the sub-surface. (a) Hatch; (b) Borders.

3.3. Strategies to reduce residual porosity

3.3.1. Utilization of high focus offset

Residual porosity was directly related to an excess of energy density in overlaps of fields and borders caused by the stop of the laser. It is well-known that offset distance or focus offset parameter greatly determines energy density and laser interaction in laser manufacturing processes. The focus offset describes the relative position of laser focal plane with respect to the top surface of powder layer (Fig. 6) and it changes the local applied energy within the laser beam spot (Ec (2) in Fig. 6). Positive focus offset implies the distance in which the laser is introduced in the sample. The increase of focus offset gives rise to the increase of the spot size, which reduces the local applied energy density but increases the beam-powder interaction time. On the one hand, a decrease in energy density will result in a temperature drop, but on the other hand, an increase in beam-powder interaction time will lead to a temperature rise. The net effect is a decrease in the overall temperature because the effect of energy density well exceeds that of the beam interaction time (Xu et al. 2015). In this study, the intensity of the laser was reduced by means of increasing the focus offset (positive focus offset values).

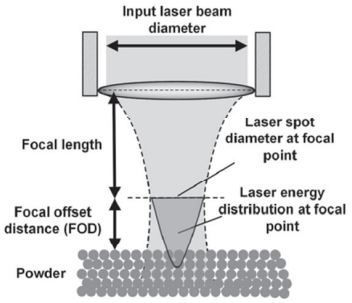

$$E = \frac{4P}{\pi \cdot v \cdot D^2} \qquad (2)$$

E = local applied energy
P = laser power
v = laser scanning velocity
D = laser spot size of a circular beam

Fig. 6. Schematic diagram showing the relative position of laser focal plane and surface of powder layer and laser energy density equation which includes influence of laser spot size (Xu et al. 2015).

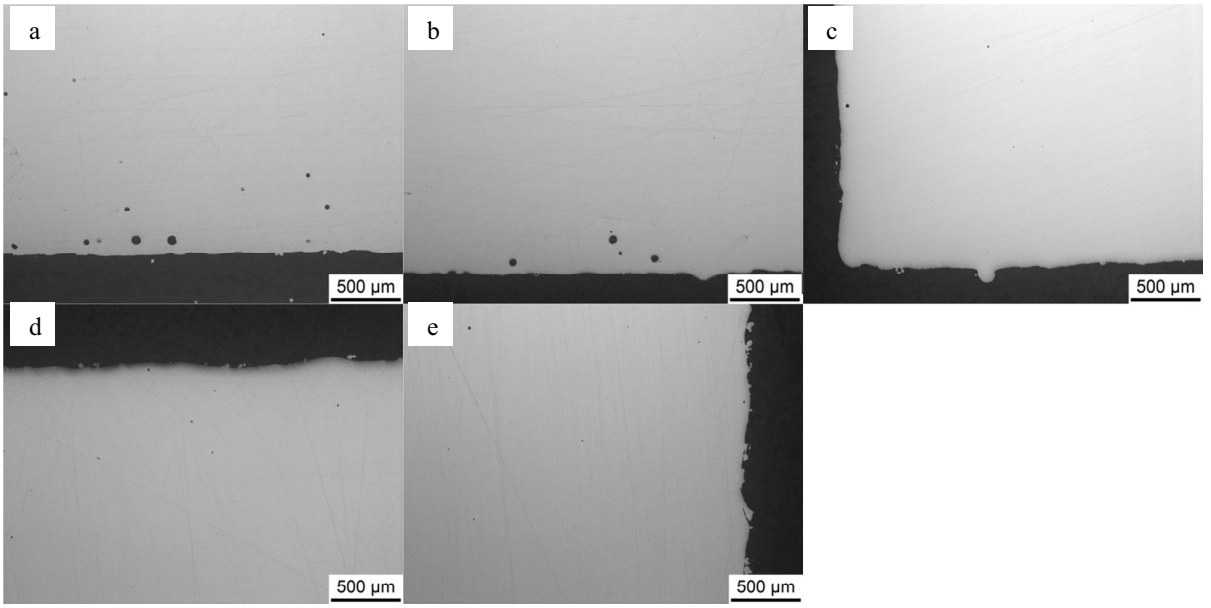

Fig. 7. Porosity obtained with increase focus offset. (a) 4 mm focus offset; (b) 6 mm; (c) 8 mm; (d) 10 mm; (e) 12 mm.

Focus offset was increased from 4 mm to 12 mm in steps of 2 mm in samples without borders and built employing long stripes. In this manner, the laser only stopped in borders and pore analysis was focused there. The process parameters used working with beam focused close to the surface were adapted. The scanning speed was reduced at high focus offsets, in order to avoid the presence of lack of fusion defects due to insufficient energy density. Micrographs of Fig. 7 (a)–(e) show the improvement obtained in porosity when employing focus offsets higher than 8 mm.

The strategy of using high focus offset was transferred to samples processed with normal stripes, composed of several in plane overlapping fields in each layer and manufactured with borders, in order to verify its effectiveness in reducing the porosity both in the hatch and in borders. A combination of high focus offset value and optimum scanning speed resulted in optimized density in the whole cube (close to 99.95%), only isolated and scattered pores were found (Fig. 8).

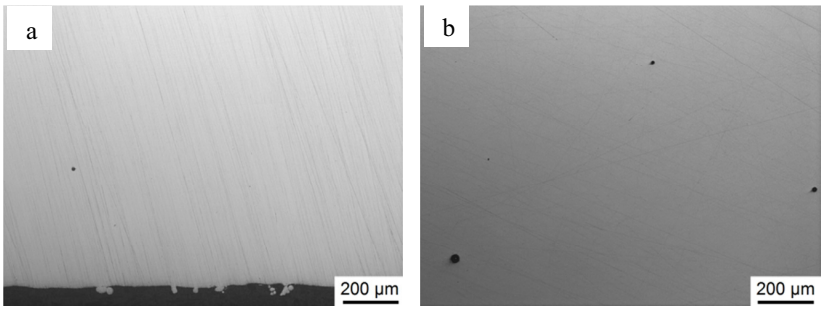

Fig. 8. Micrographs of borders (a) and hatch (b) of cubes manufactured with high focus offset (10 mm) and low scanning speed.

3.3.2. Skywriting strategy

As it is explained in the bibliography, typical scanning pattern comprises a beam following a meandering path as it progresses along the part (Fig. 9 (a)). Laser movement which determine the remote laser scanning are controlled with high accuracy by galvanometer electro-optical system. Because meandering or serpentine pattern has curved portions, the beam will have periods of acceleration and deceleration at these critical curved points (Moylan et al. 2014). That is, during scanning a certain time is needed to accelerate the mirrors to the desired speed along required

direction. This is due to inertia of galvanometer mirrors used for scanning. During this time the laser beam covers some distance in which the speed is not constant and consequently more energy input is locally introduced. That means that more energy is applied in borders and in the limits between the fields in which the part is divided, than in the rest of the part. If the skywriting function is activated, the laser beam will be switched off during the curved (accelerating and decelerating) movement and will only be on during the linear portion. In this way, it is ensured that the electro-optical system has reached the desired speed before the beginning of laser exposure. The retardation phase begins at the end of the linear part where the laser is switched off. The operating mode of the skywriting is schematically represented in Fig. 9 (b) (Manfredi et al. 2014). The skywriting avoids long interaction time between the laser and powder.

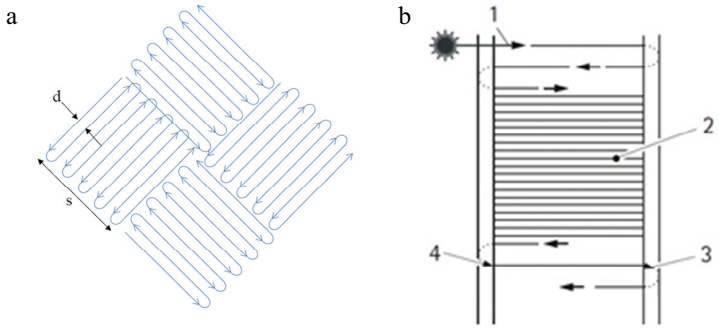

Fig. 9. (a) Schematic of the core exposure pattern; (b) 1 - Scanning vector (solid line); the skywriting is represented by the dashed line.

The effect of skywriting was studied in samples manufactured without borders and with long stripes and observing porosity at borders. In Fig. 10 (a), (b), (c) and (d) a comparison between cubes manufactured with and without skywriting is performed, where micrographs from the hatch and borders are shown. It is evident the significant improvement when the skywriting function is activated. In addition, the high quality previously observed in the hatch for the same process parameters was kept. Relative densities higher than 99.96% were obtained in the hatch.

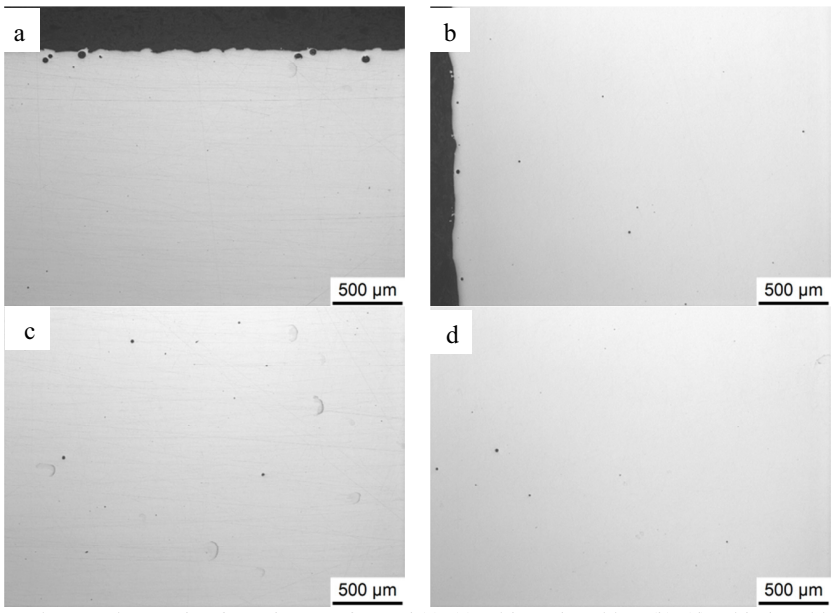

Fig. 10. Micrographs of samples manufactured (a), (c) Without skywriting; (b), (d) With skywriting.

The skywriting effectiveness was also demonstrated in samples manufactured with chessboard strategy (Figure 11 (a) and (b)). From these micrographs is evident the enhanced density in hatch, where very few pores appear and these are very small (<30 µm). The density is improved from 99.42% to 99.98% with skywrtiting. It is worth noting that with skywriting focused beam was used to build these samples.

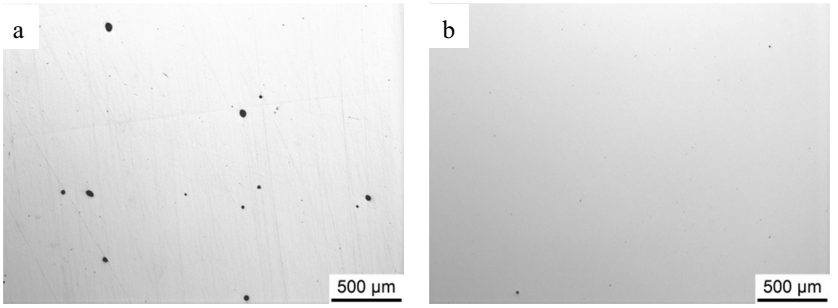

Fig. 11. Micrographs of samples manufactured. (a) Without skywriting; (b) With skywriting.

Finally, the evolution of relative density of samples with energy density is plotted in Fig. 12, where the influence of enabling skywriting function is shown. The skywriting allows reducing the residual porosity along the entire process window, with relative density values up to 99.95%.

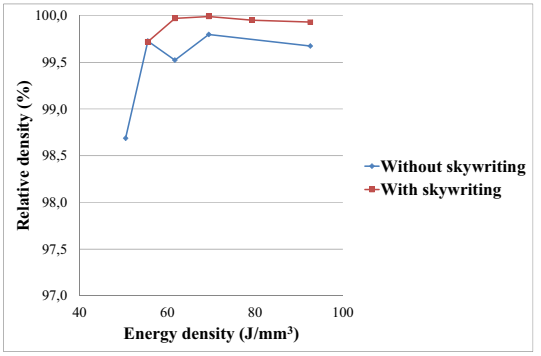

Fig. 12. Comparison of the evolution of the relative density with applied energy density of cubes manufactured with and without skywriting.

4. Conclusions

A residual porosity has been observed in Inconel 718 parts manufactured by SLM within the optimum process window. This residual porosity does not depend on the standard process parameters. On the contrary, it has been demonstrated that these pores are concentrated at specific points. These points, which are prone to contain pores are the starting and finishing of the laser scanning tracks and borders where higher energy density can concentrate. Laser start and stop events can occur in the hatch if common short stripes or chessboard strategies are employed. This has been demonstrated manufacturing cubes with long stripes where the laser only stops in borders and observing that in that case all the pores are concentrated near the surface and minimal porosity is present in the hatch. It has also been proved that the porosity is reduced considerably increasing the focus offset up to 8-10 mm. In this way, the beam is introduced in the sample and the intensity is reduced, decreasing the accumulation of energy when laser stops.

Additionally, this work describes the importance of using skywriting function for getting the highest relative density standards. Activation of this function is required in order to avoid reported residual porosity when working with very focused laser beams.

Since skywriting and focus offset have a great impact on resulting residual porosity, special attention must be paid to the activation and calibration of this function and machine set-up. Experimental procedure for checking

skywriting performance and activation as well as defocus offset can be derived form this work which is based on the analysis of porosity after working with long stripes.

References

Aboulkhair, N.T. et al., 2014. Reducing porosity in AlSi10Mg parts processed by selective laser melting. Additive Manufacturing, 1-4.

Alvarez, P. et al., 2016. Design Against Distortion of SLM Parts Based on Simplified Numerical Modelling Methodologies. Fraunhofer Direct Digital Manufacturing Conference 2016.

Averyanova, M., Bertrand, P. & Verquin, B., 2010. Effect of Initial Powder Properties on Final Microstructure and Mechanical Properties of Parts Manufactured By Selective Laser Melting. Proceedings of the 21st International DAAAM Symposium, 21(1).

Buchbinder, D. et al., 2011. High Power Selective Laser Melting (HP SLM) of Aluminum Parts. Physics Procedia, 12.

Chivel, Y., 2014. Ablation phenomena and instabilities under laser melting of powder layers. 8th International Conference on Photonic Technologies LANE 2014.

Dahotre, N.B. & Harimkar, S.P., 2008. Laser fabrication and machining of materials, New York, USA: Springer.

Gong, H. et al., 2012. Effect of defects on fatigue tests of as-built Ti-6Al-4V parts fabricated by Selective Laser Melting. Solid freeform fabrication symposium, 2012.

Gong, H., 2013. Generation An Detection Of Defects In Metallic Parts Fabricated By Selective Laser Melting And Electron Beam Melting And Their Effects On Mechanical Properties. University of Louisville, (December).

Gu, H. et al., 2013. Influences of Energy Density on Porosity and Microstructure of Selective Laser Melted 17-4PH Stainless Steel. Journal of Chemical Information and Modeling, 53(9).

Jia, Q. & Gu, D., 2014. Selective laser melting additive manufacturing of Inconel 718 superalloy parts: Densification, microstructure and properties. Journal of Alloys and Compounds, 585.

Kempen, K. & L. Thijs , E. Yasa, M. Badrossamay, W. Verheecke and J.-P. Kruth, D., 2011. Process Optimization and Microstructural Analysis for Selective Laser Melting of AlSi10Mg.

Kurzynowski, T. et al., 2012. Parameters in Selective Laser Melting for processing metallic powders. Advances in Slow and Fast Light V, 8239.

Louvis, E., Fox, P. & Sutcliffe, C.J., 2011. Selective laser melting of aluminium components. Journal of Materials Processing Technology, 211(2).

Manfredi, D. et al., 2014. Additive Manufacturing of Al Alloys and Aluminium Matrix Composites (AMCs). Light Metal Alloys Applications.

Moylan, S. et al., 2014. An additive manufacturing test artifact. Journal of Research of the National Institute of Standards and Technology, 119.

Olakanmi, E.O., 2013. Selective laser sintering/melting (SLS/SLM) of pure Al, Al–Mg, and Al–Si powders: Effect of processing conditions and powder properties. Journal of Materials Processing Technology, 213(8).

Thijs, L. et al., 2010. A study of the microstructural evolution during selective laser melting of Ti–6Al–4V. Acta Materialia, 58(9).

Xiao, R. & Zhang, X., 2014. Problems and issues in laser beam welding of aluminum–lithium alloys. Journal of Manufacturing Processes, 16(2).

Xu, W. et al., 2015. Ti-6Al-4V Additively Manufactured by Selective Laser Melting with Superior Mechanical Properties. JOM, 67(3).